redin Revista Facultad de Ingeniería, Universidad de Antioquia, No.87, pp. 41-49, 2018

# Evaluation of the effect of the synthesis method on the performance of manganese spinel as cathode material in lithium-ion batteries

## Evaluación del efecto del método de síntesis sobre el desempeño de la espinela de manganeso como material de cátodo en baterías de ion-litio

**Lina Maria Uribe-Grajales[1], Ferley Alejandro Vásquez-Arroyave[1*], Jorge Enrique Thomas[2], Jorge Andrés Calderón-Gutiérrez[1]**

[1]Centro de Investigación, Innovación y Desarrollo de Materiales – CIDEMAT, Facultad de Ingeniería, Universidad de Antioquia. Calle70 # 52 – 21. C. P. 0550010. Medellín, Colombia
[2]Instituto de Investigaciones Fisicoquímicas Teóricas y Aplicadas (INIFTA), Facultad de Ciencias Exactas, Universidad Nacional de La Plata. CCT La Plata-CONICET CC 16, Suc. 4, 1900, B1904DPI, La Plata, Argentina

**ARTICLE INFO:**
Received November 17, 2017
Accepted April 12, 2018

**KEYWORDS:**
Lithium-ion battery, Manganese spinel, Solid-state synthesis, Sol-gel, Elemental substitution

Batería ion-litio, Espinela de manganeso, Síntesis en estado sólido, Sol-gel, sustitución elemental

**ABSTRACT:** Spinel-structured lithium manganese oxide $(LiMn_2O_4)$ has been successfully used as a cathode material for various lithium batteries. To improve the capacity and increase the discharge potential of the battery, transition metals are commonly added to the spinel as dopants or as a substitute for manganese. This can also confer stability on the structure of the cathode material. In this work, the production and performance of spinel $LiMn_2O_4$ (LMO) and $LiNi_{0.5}Mn_{1.5}O_4$ (LNMO) by solid-state and sol-gel synthesis methods were studied. Synthetized (LMO) and (LNMO) materials were characterized by Raman spectroscopy and X-ray diffraction (XRD) to verify the formation of a spinel-like structure. It was corroborated that both synthesis methods can produce an adequate spinel structure. SEM analyses showed that in general, spinel take an octahedral form. The particle size changes according to the synthesis method used. Lower particle sizes were obtained by sol-gel. The electrochemical characterization demonstrates that solid-state synthesis generates compounds with greater purity and crystallinity, which induces a greater capacity of lithium ion intercalation. The addition of nickel to the spinel increases the discharge potential of the cathode by 0.5V.

**RESUMEN:** Los óxidos de manganeso con estructura tipo espinela $(LiMn_2O_4)$ han sido utilizados con éxito como materiales de cátodo para las baterías de ion-litio. Para mejorar la capacidad e incrementar el potencial de descarga de la batería, comúnmente se han adicionado metales de transición a la espinela, como dopantes o sustituyentes del manganeso. Esto puede conferirle también estabilidad a la estructura del material de cátodo. En este trabajo se evaluó la obtención y el desempeño de las espinelas de $LiMn_2O_4$ (LMO) y $LiNi_{0.5}Mn_{1.5}O_4$ (LNMO) obtenidas por procesos de síntesis en estado sólido y sol-gel se estudiaron. Los materiales sinterizados de (LMO) y (LMNO) se caracterizaron por espectroscopia Raman y difracción de rayos X (DRX) para evidenciar la formación de la estructura tipo espinela. Fue corroborado que mediante ambos métodos de síntesis se puede producir una estructura de espinela adecuada. El análisis SEM mostró en general que la espinela adquiere una forma octahedral. El tamaño de partícula cambia de acuerdo al método de síntesis empleado, obteniendo un menor tamaño de partícula en la síntesis por sol-gel. La caracterización electroquímica demuestra que la síntesis por estado sólido genera componentes con mayor pureza y cristalinidad, los cuales generan una mayor capacidad de intercalación de iones litio. La adición de níquel a la espinela incrementa el potencial de descarga del cátodo en 0.5V.

## 1. Introduction

Lithium-ion batteries are characterized by their high specific energy, high efficiency and long lifetime. Li has the most negative standard reduction potential of all

* Corresponding author: Ferley Alejandro Vásquez Arroyave
E-mail: ferley.vasquez@udea.edu.co
ISSN 0120-6230
e-ISSN 2422-2844



DOI: 10.17533/udea.redin.n87a06

elements, allowing Li-ion based batteries to have the highest possible cell potential. In addition, lithium is the lightest metal so with the LIBs considerable savings of mass can be obtained [1].

With technological advances in electric transport systems and the massification of growth in photovoltaic energy generation systems, energy storage devices require greater load density and useful life. However, the expansion of lithium-ion battery technology for these applications remains problematic due to issues such as safety, cost and availability of materials.

Spinel $LiMn_2O_4$ (LMO) is commonly used as a cathode active material in lithium ion batteries due to the low cost, environmental friendliness and high level of safety during the intercalation of lithium ions in its structure. To improve capacity and increase the spinel discharge potential, transition metals are added as dopant or substituent elements, which can also confer stability on the structure of the cathode material [2]. The most common element added to the LMO spinel for cathode usage is nickel. This is the one that has drawn the most attention due to the fact that nickel confers higher charge density by increasing the voltage of the battery to values of 4.7 V $vsLi^+/Li$, and the capacity to about $130mAhg^{-1}$. This gives a specific energy of about $610Whg^{-1}$, higher than many marketed compounds. Other doping or substitute elements such as iron, cobalt, chromium, titanium, aluminum, vanadium and niobium have been added as dopants and co-dopants in manganese spinels. This has shown that many of these elements favor the formation of a disordered structure with spatial groups of $Fd\bar{3}m$, which increases the cathode voltage, provides superior velocity response during cycling and improves the stability of the cathode structure. The addition of iron, while improving the electrical conductivity of the structure, may reduce the cathode voltage [2–4].

Current needs with respect to transport, renewable energies generation, mobile communication and electronic devices require batteries with greater density of energy storage [5]. Spinel structure presents good characteristics to increase the energy capacity and working voltage of batteries. However, it is also necessary to develop spinel-like structures with greater stability and less lithium-ion intercalation time, which must be accompanied by economic and environmentally friendly synthesis processes [6, 7].

Low cost synthesis methods aimed at improving the performance of the cathode materials in terms of capacity, electric response rate and service life can be developed based on knowledge of the structural and chemical behavior of the spinel during cycling and the effect of the addition of dopant or substituent elements [4, 8, 9].

Manganese spinels can be synthesized in wet chemistry by mixing the precursors in aqueous or organic solvents to obtain active materials with good stability [10]. Also, they can be obtained quickly and with less process steps by burning the precursors directly into the flame [11]. Usually, synthesis methods of manganese spinel such as sol-gel and solid-state have demonstrated a greater potential for application in batteries due to their low cost and improved properties in terms of load capacity and response speed during cycling [12]. These properties are directly related to the purity and morphology of the active cathode material [13]. Despite the extensive literature related to manganese spinel synthesis methods and their effect on the electrochemical properties of the material, it is necessary a better understanding of the effect of synthesis route on the composition, morphology and particle size of pure lithium-manganese spinel and nickel-manganese spinel. [12, 13].

This work aims to assess the effect of the most commonly used methods for manganese spinel synthesis, solid-state and sol-gel. Also, the addition of nickel by both synthesis methods on the performance of the cathode material for lithium-ion batteries was assessed. The formation of a spinel-like structure and purity after synthesis was evaluated by X-ray diffraction (XRD) and Raman spectroscopy. The size and morphology of the materials were assessed by Scanning Electron Microscopy (SEM), while the electrochemical performance was evaluated by cyclic voltammetry, galvanostatic charge-discharge cycles and electrochemical impedance spectroscopy (EIS).

## 2. Experimental

### 2.1 Materials

Lithium-manganese spinels $LiMn_2O_4$ (LMO) and nickel-substituted $LiNi_{0.5}Mn_{1.5}O_4$ (LNMO) were synthesized by solid-state and sol-gel methods. Reactive grade reagents like lithium acetate dihydrate $(LiC_2H_3O_2 - 2H_2O)$ and nickel nitrate hexahydrate $(NiNO_3 - 6H_2O)$ from Alfa-Aesar and manganese acetate tetrahydrate $(MnC_2H_3O_2 - 4H_2O)$ from Sigma-Aldrich, were used as precursors.

Solid-state synthesis was performed following the general guidelines described in [14]. The precursors were mixed in stoichiometric amounts for 5 min. in an agate mortar. The mixture was burned at 900 °C for 24h in air, followed by successive heating at 700 °C for 24h, at 650 °C for 24h and finally at 600 °C for 48h. During sol-gel synthesis, the precursors were mixed in stoichiometric amounts to form a solution with citric acid $\left(0.01molL^{-1}\right)$.

The pH of the solution was adjusted to 6.8 by adding $NH_4OH$. The solution was completed to a total volume of 25 mL and then evaporated at 75 °C until a wet gel consistency was obtained. Following this, the gel was allowed to stand for 24h and then dry at 90 °C under vacuum for 12h. The obtained solid was burned at 450 °C for 5h in air. Finally, the obtained powder was calcined at 850 °C for 18h (previous studies were done to determine the adequate temperature for the thermal treatment).

## 2.2 Characterization

The synthesized spinels were characterized by X-ray diffraction (XRD) using a PANalytical reference equipment with an X-ray source of cobalt. The scan was performed considering a $2\theta$ between 10 - 90°. The flush angle between the specimen holder and the detector was set at 5°. Raman spectroscopy measurements were performed using a Nikon model BX41 microscope with X50 objective and a high resolution Labram HR model from Horiba Jobin Yvon under the following conditions: a focal length of 800mm, CCD detector with 1024x256 pixel resolution, 632.81$cm^{-1}$ He/Ne laser, D2 filter, 1000µm hole, a sweep range of 100-2000$cm^{-1}$. The morphology of the synthesized particles was characterized by Scanning Electron Microscopy (SEM) using JEOL JSM 6490 LV equipment.

## 2.3 Electrochemical measurements

All the samples were characterized by cyclic voltammetry, galvanostatic charge-discharge cycles and electrochemical impedance spectroscopy. Three electrode "T" type cells in a controlled temperature room at 25°C were used. Lithium foil was used as the counter and as a reference electrode. All the potentials reported in this paper are referred to the Li+/Li redox potential. The working electrodes were composed of 80 wt% active material, 10 wt% conductive carbon additive (Super P®), and 10 wt% PVDF binder. A solution 1.5 M LiPF6 in a 1:2 w/w mixture of EC:DMC was used as electrolyte, and cell assembly was carried out in a MBraun glove box with moisture and oxygen concentrations below 1ppm.

The charge-discharge cycling behavior of the electrodes was studied using a Multichannel Arbin BT-2000 station. The electrodes were charged and discharged at a constant current of C/2 (50 mA $g^{-1}$) with voltage limits of 2.7 V and 5.2 V. Cyclic voltammetry (CV) and electrochemical impedance spectroscopy (EIS) were performed using an Autolab PGSTAT302N potentiostat. The CV experiments were carried out between 2.7V and 5.2V at 0.1mV/s. The EIS test was performed at 50% of state of charge (SOC) using a potentiostatic method at the open circuit potential (OCP) of each SOC, with an amplitude of 10mV and frequencies ranging from 100 kHz to 50 mHz.

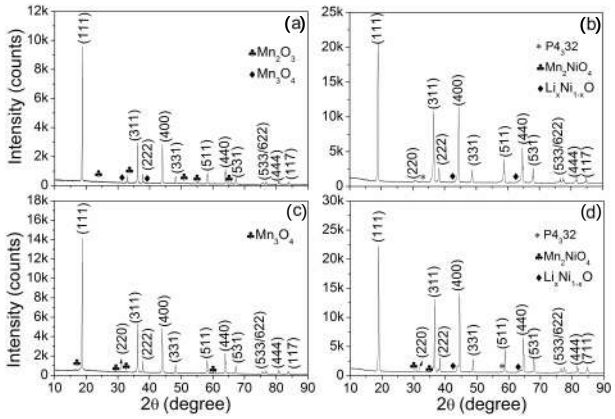


**Figure 1** DRX patterns of spinel materials obtained by solid state: (a) $LiMn_2O_4$ and (b)$LiNi_{0.5}Mn_{1.5}O_4$. Sol-gel: (c) $LiMn_2O_4$ and (d)$LiNi_{0.5}Mn_{1.5}O_4$

# 3. Results and Analysis

## 3.1 Materials characterization

Figure 1 presents the diffraction patterns of LMO and LMNO materials obtained by solid-state and sol-gel methods. The pattern of the solid-state LMO (Figure 1a) is assigned to a cubic structure in a space group $Fd\bar{3}m$, where lithium ions occupy the 8a sites, manganese ions occupy the 16d sites and oxygen ions occupy the 32e sites. In this LMO sample, the presence of impurities of manganese oxides, such as $Mn_2O_3$ and $Mn_3O_4$, in amounts of 5.4% and 3.4% respectively, were observed. The qualification and quantification of the phases was obtained with Rietveld refinement, obtaining a goodness of fit of 1.40. Since the adjustment of the Rietveld refinement had a "goodness of fit" below 4 it can be said that the adjustment is adequate and represents the phases mentioned. The results obtained are consistent with other XRDs performed in spinel synthesized by hydrothermal methods [15].

The pattern of the LNMO material obtained by solid-state (Figure 1b) is assigned to a cubic structure in a space group $P4_332$, where the lithium ions occupy the 8a sites, the manganese ions occupy the 12d sites, the nickel occupies 4a sites and oxygen occupies positions 8c and 24e [16, 17]. In this sample, impurities of $Li_xNi_{1-x}O$ (which is the most commonly reported impurity for this spinel) were also observed, in an amount of 8.7% [12, 18–22]. In addition, non-lithiated state spinel $Mn_2NiO_4$ was obtained in an amount of 7.6%. This refinement was obtained with a goodness of fit of 2.4.

The pattern for the LMO material obtained by sol-gel method (Figure 1c) is assigned to a cubic structure, in a space group $Fd\bar{3}m$. This sample contains impurities of manganese oxide, $Mn_3O_4$ in an amount of 3.4%. This refinement was obtained with a goodness of fit of 1.91. The pattern of LNMO obtained by sol-gel (Figure 1d) is assigned to a cubic structure in a spatial group $P4_33_2$. The sample was obtained with the impurity $Li_xNi_{1-x}O$ in an amount of 10.8%. Additionally, non-lithiated state spinel $Mn_2NiO_4$ is present as an impurity in an amount of 3.6%. This refinement was obtained with a goodness of fit of 2.02. The XRD results of the samples are consistent with previous reports of XRD performed on nickel-doped spinels, showing the formation of an ordered structure of LNMO spinel (with spatial groups $P4_33_2$) and a disordered structure of LMO spinel (with spatial groups $Fd\bar{3}m$). Additionally, there is a shift of $2\theta$ angle to superior values of the (440) peak when nickel is incorporated into the structure. The peak (440) moves from a $2\theta$ angle value of 63.9° for the spinel without nickel to a $2\theta$ angle value of 64.9° for the spinel with nickel insertion. When nickel is added to the spinel structure the manganese atoms are partially replaced by nickel atoms and there is a partial deformation of the structure by the reduction of the network parameter [23, 24].

Figure 2 shows the Raman spectra of the synthesized samples. In the spectra of the LMO material (Figures 2(a) and 2(c)), the characteristic band located at around 625 $cm^{-1}$ of the $Mn-O$ bond is presented. This band corresponds to the octahedric group of $MnO_6$ in the $A_{1g}$ mode. The bands at 582 and 365 $cm^{-1}$ are assigned to $T_{2g}$(3) and $T_{2g}$(1) predicted by group theory for cubic compound [25, 26]. Additionally, the band at 666 $cm^{-1}$ is related to the $Mn-O$ vibration in the $Mn_3O_4$ impurities [27].

The Raman spectra of the LNMO samples (Figure 2(b)) and 2(d)) change respect to LMO samples since the introduction of the $Ni^{2+}$ ions into the spinel's network induces additional bonds and consequently increases the number of bands in the Raman spectra of the spinel. The Raman spectra of the LNMO exhibit bands located at 409 and 500 $cm^{-1}$ for the spinel synthesized by solid state method and bands at 412 and 493 for the spinel synthesized by sol-gel which are associated with the vibrations of $Ni-O$ groups [28]. The Raman spectra of the LMNO spinel synthesized by sol-gel exhibit bands located at 164, 215, 584 and 634 $cm^{-1}$, corresponding to symmetric vibrations of $Mn-O$ in the $MnO_6$ octahedral sites [21, 28]. The substituted nickel spinels synthesized by solid-state show more defined and higher intensity bands than those observed for the other samples, which could be associated with the superior purity of the phase [29–32]. The LMO spinels synthesized by solid-state and sol-gel methods present spectra related to a structure with characteristic vibrations of $Fd\bar{3}m$ spatial groups [30, 31]. On the other hand, the LMNO spinel obtained by solid-state shows a spectrum with characteristic bands associated with $P4_33_2$ spatial groups (see Figure 2d) [30, 33].

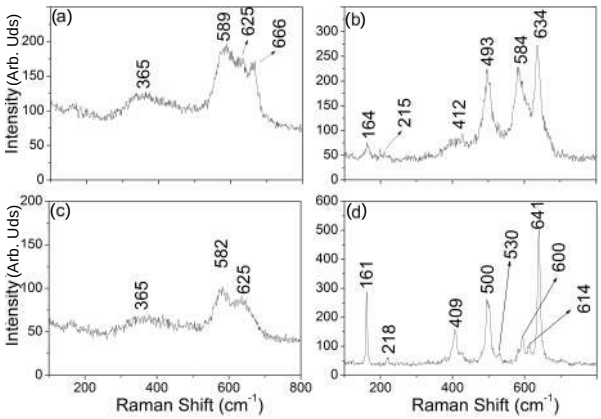


**Figure 2** Raman spectra of the spinel materials obtained by sol-gel: (a) $LiMn_2O_4$ and (b)$LiNi_{0.5}Mn_{1.5}O_4$. Sol-gel: (c) $LiMn_2O_4$ and (d)$LiNi_{0.5}Mn_{1.5}O_4$

The LNMO spinel synthesized by sol-gel shows characteristic vibration bands of both, the order and disorder phases [30, 33–35]. Figure 3 shows the SEM images of spinel materials obtained by solid-state and sol-gel methods. As can be seen, the LMO and LNMO spinels obtained by both methods exhibit octahedral morphology. This octahedral structure is one of the different structures that manganese spinels can exhibit. Other manganese spinel structures such as spherical, truncated (octahedral with flattened tips), cubic and octahedral morphologies have been reported in the literature with higher capacity and rate capability [36, 37]. It can also be observed that the crystal size of the LMO spinel depends on the synthesis method used, with larger crystal size being obtained during solid-state synthesis than in the sol-gel method. Due to the long time and high temperatures of synthesis in the solid-state method, the crystals obtained by this method are larger and more ordered. Conversely, as the temperatures and processing times of the sol-gel method are lower than those of the solid-state, it is expected that smaller and less ordered particles will be obtained after the process by sol-gel. Additionally, for the solid-state method the synthesized samples have shown higher purity than in the sol-gel method. In the case of the LNMO spinel synthesized by solid-state, a higher ability to intercalate lithium ions is expected due to the superior purity of the phase.

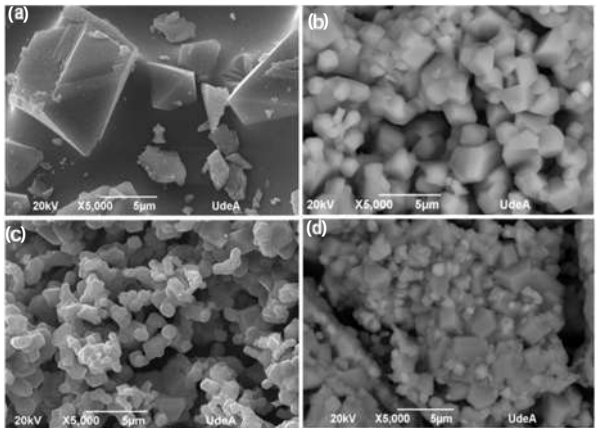


**Figure 3** SEM images of spinel materials obtained by solid state: (a) $LiMn_2O_4$ and (b)$LiNi_{0.5}Mn_{1.5}O_4$. Sol-gel: (c) $LiMn_2O_4$ and (d)$LiNi_{0.5}Mn_{1.5}O_4$

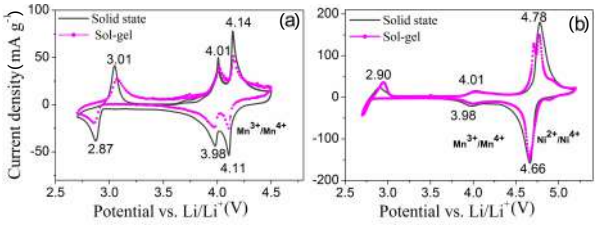


**Figure 4** Cyclic voltammetry performed to the lithium-manganese samples obtained by solid state and sol-gel methods. (a) $LiMn_2O_4$ and (b) $LiNi_{0.5}Mn_{1.5}O_4$

## 3.2 Electrochemical performance

Figure 4 shows the cyclic voltammetries of samples obtained by solid-state and sol-gel methods. The voltammograms reveal the good reversibility of materials for the intercalation of Li ions in a potential range from 2.5 to 5.2 V, which is in agreement with literature reports [38]. For the spinel LMO (Figure 3a) three oxidation peaks and three reduction peaks are observed.

The two peaks observed at 4.01 and 4.14V vs. $Li/Li^+$ correspond to the two-stage process for the extraction of lithium. The anodic and cathodic peaks observed at the low potential of 3.01V and 2.87V vs. $Li/Li^+$, respectively, correspond to the reversible phase transformation of $LiMn_2O_4 \rightarrow Li_2Mn_2O_4$ [38].

In the spinel LNMO, Figure 4(b), there are three pairs of oxidation/reduction peaks. The peaks around 4.78V and 4.66V vs. $Li/Li^+$ correspond to the reversible oxidation-reduction process of nickel(II) $Ni^{2+} \leftrightarrow Ni^{3+} \leftrightarrow Ni^{4+}$) [39, 40]. On the contrary, in the spinel synthesized by solid state method was observed an asymmetric peak around the 4.7V, the asymmetry of the redox peaks can be related to an overlap of the second peak since the spinel synthesized by solid-state contains a lower quantity of disordered phase [41]. The small shoulder at 4.9V is related to an intercalation process of $PF^{-6}$ ion within the graphite structure of conductive carbon present in the active material [42]. In addition, the current peaks related to the oxidation/reduction of the Mn ions are significantly lower than those related to the LMO spinel due to the substitution of Mn by Ni ions in the spinel structure. The discharge potentials exhibited by the synthesized spinels show similar values to those reported in other work performed on nickel-doped spinels and synthesis by solid-state [28]. The presence of two oxidation/reduction processes in the LMO and LMNO spinels at voltages around 4V was related with manganese oxidation-reduction process [3, 28, 43]. On the other hand, the manganese oxidation-reduction peak at 4V confirms the presence of disordered spinel in the active material.

The current peak around 3 V remains intact in all samples, which indicates that the reversible phase transformation was not affected by the addition of nickel to the spinel structure.

A higher current peak indicates higher kinetics of oxidation-reduction processes, which may be associated with a higher intercalation rate of lithium ions in the structure. Consequently, as higher current peaks in the oxidation/reduction processes were observed in both LMO and LMNO solid-state synthesized spinels than those observed in sol-gel spinels, higher kinetics of lithium intercalation is expected for spinels synthesized by the solid-state method. The better lithium intercalation kinetics observed in the solid-state synthesized spinels could be related to the higher crystallinity of their structure [44]. Furthermore, the Ni substituted spinels exhibit higher current peaks in the redox processes, which indicates higher intercalation speed of lithium ions. Therefore, higher energy capacity is expected for this spinel material.

The discharge characteristic curves of synthesized cathode materials are shown in Figure 5. It is observed that the LMO samples present a plateau at approximately 4.1 V, obtaining slightly greater capacity for the sample synthesized by sol-gel. The LNMO spinels present a plateau at around 4.7 V. The higher discharge potential in the LMNO materials than the LMO materials is related to the incorporation of nickel into the spinel structure, which partially replaced the manganese. This is due to the fact that the redox process of the nickel ions $(Ni^{2+}/Ni^{4+})$ have higher electrochemical potential than the redox process of the manganese ions $(Mn^{3+}/Mn^{4+})$. This increases the cathode potential during the lithium ion intercalation into the spinel. As can be seen in Figure 5, during the discharge at a capacity of $80mAhg^{-1}$,

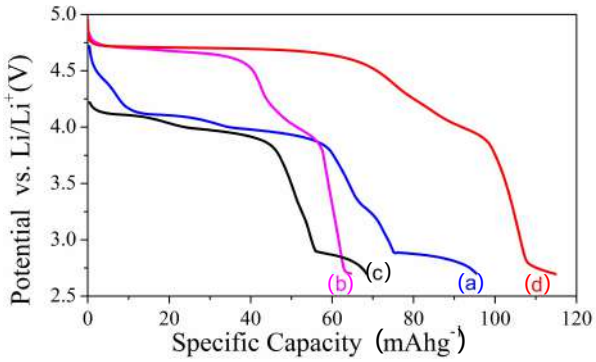


**Figure 5** Discharge capacity vs. voltage for synthesized cathode materials. Sol-gel method: (a) $LiMn_2O_4$ (b) $LiNi_{0.5}Mn_{1.5}O_4$. Solid state method: (c) $LiMn_2O_4$ and (d) $LiNi_{0.5}Mn_{1.5}O_4$. Curves were made at a constant current of C/2

it is considered that almost all of the divalent nickel ions inserted into the structure have been oxidized and the trivalent manganese ions have begun to oxidize, lowering the potential to values close to 4 V [45]. Greater discharge capacity was observed for the spinel LMNO obtained by solid-state, which could be related to the greater purity and crystallinity of this material. The solid-state synthesized spinel exhibited values of energy capacity and discharge voltage close to those reported for similar spinel synthesized by methods such as hydrothermal and electrospinning, which are higher-cost [46, 47]. Those synthesis methods require greater inputs, equipment and energy consumption; which shows that lithium-manganese spinel cathode materials can be obtained through a cheaper method without compromising the lithium ion intercalation capacity.

EIS experiments were carried out in order to investigate the effect of synthesis method and of substituting Ni ion on the interfacial resistance and diffusion coefficient of lithium ion in spinel cathode materials. Figure 6 shows the electrochemical impedance spectroscopy (Nyquist plots) performed at 50% of charge on the $LiMnO4$ and $LiNi_{0.5}Mn_{1.5}O_4$ spinels synthesized by both sol-gel and solid-state methods. For the spinels without Ni obtained by both synthesis methods (Figure 6a) and for the spinel with Ni obtained by solid-state (Figure 6b), the Nyquist diagrams show two capacitive loops formed at high and intermediate frequencies and one capacitive loop at low frequencies. The first loop at high frequencies is associated with the resistance of the passivation layer (SEI) formed on the material of the cathode. The second capacitive loop at intermediate frequencies is associated with the charge transfer at the electrode-electrolyte interface in parallel with the double-layer capacitance. The loop at low frequencies is associated with processes of diffusion of the lithium ions within the structure of the spinel. Similar impedance responses for spinel cathode materials have been reported in other works [23, 48].

Otherwise, the electrochemical impedance for nickel containing spinel synthesized by sol-gel method exhibited a different electrochemical impedance response than those observed for other spinel. As can be seen in the insert of Figure 6(b), three capacitive loops at high and intermediate frequencies and one loop at low frequencies related to the diffusion of lithium ions were observed. For this system, the second and third loops at intermediate frequencies are associated with processes of charge transfer and charging of the double-layer capacitance in two different phases, one of them being the ordered phase and the another the disordered phase. The presence of two phases with different ordering grades in the spinel $LiNi_{0.5}Mn_{1.5}O4$ obtained by sol-gel method was discussed during the analysis of Raman and CV results.

The experimental EIS diagrams obtained for the cathode materials were fitted using equivalent electrical circuits shown in Figure 7. This takes into account the resistance of the electrolyte $(R_{sol})$ in series with a characteristic RQ of the SEI, and in series with RCQ characteristic of the active material of the cathode. The characteristic RCQ of the cathode active material takes into account the charge transfer resistance $(R_{ct1})$, the double-layer capacitance $(C_{eff.dl1})$ and the lithium ion diffusion. The diffusion of the lithium ions can be represented by a constant phase element (CPE) since it occurs through the pores of the active material [49]. The capacitance of the SEI is represented by a constant phase element (CPE) because of the inhomogeneous nature of the SEI. Table 1 presents the values of the parameters used to fit the experimental EIS diagrams with the respective equivalent electrical circuit. The effective capacitances $(C_{eff})$ were calculated by the Equation 1, through the series resistance $(Rs)$ and parallel resistance $(Rp)$

$$C_{eff} = \left[ Q \left( \frac{1}{Rs} + \frac{1}{Rp} \right)^{(a-1)} \right]^{\left(\frac{1}{a}\right)} \quad (1)$$

Where "Q" is the CPE element value, "a" is the exponential term value. "Rs" represents the series resistance, and "Rp" represents the parallel resistance with the CPE element [50].

The diffusivity $(Dif)$ was calculated by the Equation 2, taking into account the capacitance at low frequencies $(C_{Dif})$, the resistance of the diffusion process $(Rw)$ measured at the limit of zero frequency and the half distance $(L/2)$ of diffusion of lithium ions within the spinel [49].

$$Dif = \frac{(L/2)^2}{Rw * C_{Dif.}} \quad (2)$$

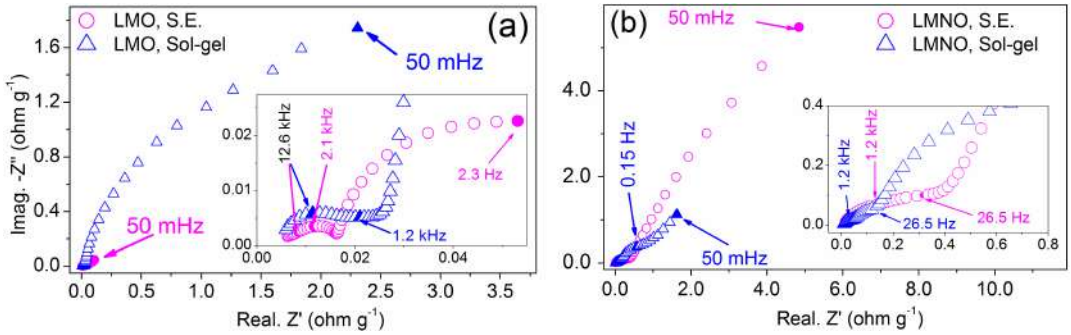


**Figure 6** Electrochemical impedance of the spinel materials synthesized by solid state and sol-gel methods performed at 50% SOC. (a) $LiMn_2O_4$ and (b) $LiNi_{0.5}Mn_{1.5}O_4$

**Table 1** Values of the parameters used to fit the experimental EIS diagrams according to the equivalent circuit shown in Figure 7

| Element | LMO-S.E | LMO- Sol gel | LNMO-S.E | LNMO- Sol gel |
|---|---|---|---|---|
| $R_{sol}$ **(ohm g)** | 6.3E-03 | 3.3E-03 | 7.0E-03 | 7.3E-03 |
| $R_{SEI}$ **(ohm g)** | 1.1E-02 | 2.3E-02 | 4.6E-01 | 4.6E-02 |
| $C_{SEI}$ **(F g$^{-1}$)** | 3.1E-03 | 2.8E-04 | 3.7E-05 | 3.7E-04 |
| $R_{ct1}$ **(ohm g)** | 4.3E-02 | 9.6E-01 | 4.6E+00 | 4.7E-01 |
| $C_{eff.dl1}$ **(F g$^{-1}$)** | 6.2E-01 | 2.3E-01 | 1.2E-01 | 8.3E-02 |
| $R_{ct2}$ **(ohm g)** | - | - | - | 1.4E-01 |
| $C_{eff.dl2}$ **(F g-1)** | - | - | - | 1.4E-02 |
| $R_w$ **(ohm g)** | 1.3E-01 | 9.2E+00 | 3.6E+01 | 8.0E+00 |
| $C_{Dif}$ **(F g$^{-1}$)** | 1.9E+01 | 1.1E-01 | 1.3E-01 | 3.5E-01 |
| **L/2 (cm)** | 5.0E-4 | 8.5E-5 | 1.4E-4 | 1.0E-4 |
| **Dif. (cm$^2$ s$^{-1}$)** | 5.9E-07 | 7.3E-09 | 8.6E-08 | 2.8E-08 |
| **Goodness of Fit** | 2.2E-04 | 8.4E-04 | 8.2E-03 | 6.1E-03 |

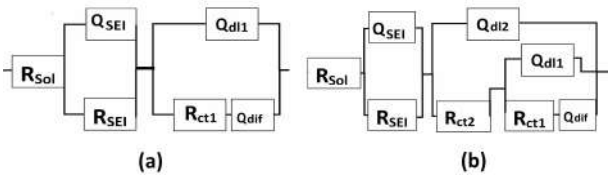


**Figure 7** Equivalent circuits used to fit the electrochemical impedance spectroscopy (EIS). (a) Spinel materials LMO synthesized by both methods and LMNO synthesized by solid state method. (b) Spinel material LMNO synthesized by sol-gel method

Similar values of solution resistance were found for the four materials. The small differences between them were due to the cell conformation. The SEI resistance shows greater values for the spinel with Ni synthesized by solid-state, which is due to the formation of a thick and compact film. The SEI resistance values found are similar to values reported in the literature for intercalation spinel materials (see Table 1) [51]. The charge transfer resistance during the lithium ions intercalation $(R_{ct1})$ exhibited greater values on spinel with Ni synthesized by solid-state, this being due to the lower electronic conductivity of the ordered structure with spatial groups $P4_332$ compared to the disordered structure with spatial groups $Fd\bar{3}m$ found in the spinel materials without Ni and with Ni synthesized by sol-gel [52–54].

The diffusivity values are consistent with the results of cyclic voltammetry of the spinel materials, in which the solid-state sintered spinel exhibits higher oxidation/reduction peaks. EIS results show that spinel materials synthesized by solid-state exhibit greater diffusivity of lithium ions within the structure, which is related to the higher crystalline order. This condition gives a higher rate of lithium intercalation of these active cathode materials. However, the insertion of Ni into the structure can reduce the diffusion of the lithium ions within the crystallites. This effect is due to the smaller atomic size of the nickel compared to the manganese, generating compression effects that distort the structure and reduce the diffusion spaces [23]. Additionally, during des-lithiation the nickel oxidation state changes from $2^+$ to $4^+$, generating a greater electrical repulsion of the lithium ions. This renders the diffusion of the lithium ions through all the crystallographic directions more difficult and increases the barrier energy for the diffusion of the lithium ions [55].

## 4. Conclusion

The structural crystallinity of solid-state spinel is greater than that the exhibited by sol-gel spinel, which facilitates the diffusivity of lithium ions into the structure. Additionally, solid-state synthesized spinel exhibits higher purity, which induces a higher capacity for the lithium ion intercalation. The insertion of Ni into the spinel favors the formation of spatial groups of P4332 which induces some ordering in the spinel with both solid-state and sol-gel synthesis methods; although, there is still Mn and most likely partial Fd3m presence in the structure. On the other hand, the LMO spinel forms spatial groups of $Fd\bar{3}m$ with less ordering. The addition of nickel as a substitute element for manganese increases the working voltage.

The lithium ion intercalation within the spinel structure containing nickel was limited by both the electrical conductivity and the diffusion of the lithium ions within crystallites. The first property was affected by the presence of an ordered structure and the second by the electrostatic forces generated by the nickel in the structure.

## 5. Acknowledgements

The authors are pleased to acknowledge the financial assistance of the "Departamento Administrativo de Ciencia, Tecnología e Innovación - COLCIENCIAS" through the project 111574558653 and the "Estrategia de Sostenibilidad de la Universidad de Antioquia".

## References

[1] G. Rayner, *Química Inorgánica Descriptiva*, 2nd ed. México, D.F: Pearson Educación, 2000.

[2] Y. S. Meng and M. E. A. Dompablo, "Recent advances in first principles computational research of cathode materials for lithium-ion batteries," *Acc. Chem. Res.*, vol. 46, no. 5, pp. 1171–1180, 2013.

[3] G. B. Zhong, Y. Y. Wang, Y. Q. Yu, and C. H. Chen, "Electrochemical investigations of the lini$_{0.45}$m$_{0.10}$mn$_{1.45}$o$_4$ (m = fe, co, cr) 5v cathode materials for lithium ion batteries," *J. Power Sources*, vol. 205, pp. 385–393, May 2012.

[4] T. F. Yi, Y. Xie, Y. R. Zhu, R. S. Zhu, and M. F. Ye, "High rate micron-sized niobium-doped limn$_{1.5}$ni$_{0.5}$o$_4$ as ultra high power positive-electrode material for lithium-ion batteries," *J. Power Sources*, vol. 211, pp. 59–65, Aug. 2012.

[5] J. H. Wesseling, E. M. Niesten, J. Faber, and M. P. Hekkert, "Business strategies of incumbents in the market for electric vehicles: Opportunities and incentives for sustainable innovation," *Bus. Strateg. Environ.*, vol. 24, no. 6, pp. 518–531, Dec. 2015.

[6] D. L. Wood, J. Li, and D. Claus, "Prospects for reducing the processing cost of lithium ion batteries," *J. Power Sources*, vol. 275, pp. 234–242, Feb. 2015.

[7] Y. C. Jin, M. I. Lu, T. H. Wang, C. R. Yang, and J. G. Duh, "Synthesis of high-voltage spinel cathode material with tunable particle size and improved temperature durability for lithium ion battery," *J. Power Sources*, vol. 262, pp. 483–487, Sep. 2014.

[8] T. F. Yi, J. Mei, and Y. R. Zhu, "Key strategies for enhancing the cycling stability and rate capacity of $LiNi_{0.5}Mn_{1.5}O_4$ as high-voltage cathode materials for high power lithium-ion batteries," *J. Power Sources*, vol. 316, pp. 85–105, Jun. 2016.

[9] L. C. *et al.*, "Life modeling of a lithium ion cell with a spinel-based cathode," *J. Power Sources*, vol. 221, pp. 191–200, Jan. 2013.

[10] J. W. W. *et al.*, "One-step synthesis and effect of heat-treatment on the structure and electrochemical properties of lini$_{0.5}$Mn$_{1.5}$O$_4$ cathode material for lithium-ion batteries," *Electrochim. Acta*, vol. 133, pp. 515–521, Jul. 2014.

[11] X. Zhang, H. Zheng, V. Battaglia, and R. L. Axelbaum, "Flame synthesis of 5 v spinel-$LiNi_{0.5}Mn_{1.5}O_4$ cathode-materials for lithium-ion rechargeable-batteries," *Proc. Combust. Inst.*, vol. 33, no. 2, pp. 1867–1874, 2011.

[12] L. H. Chi, N. N. Dinh, S. Brutti, and B. Scrosati, "Synthesis, characterization and electrochemical properties of 4.8V $LiNi_{0.5}Mn_{1.5}O_4$ cathode material in lithium-ion batteries," *Electrochim. Acta*, vol. 55, no. 18, pp. 5110–5116, Jul. 2010.

[13] C. Zhu, A. Nobuta, G. Saito, I. Nakatsugawa, and T. Akiyama, "Solution combustion synthesis of $LiMn_2O_4$ fine powders for lithium ion batteries," *Adv. Powder Technol.*, vol. 25, no. 1, pp. 342–347, Jan. 2014.

[14] E. H. *et al.*, "Oxygen-Release-Related Thermal Stability and Decomposition Pathways of $Li_xNi_{0.5}Mn_{1.5}o_4$ Cathode Materials," *Chem. Mater.*, vol. 26, no. 2, pp. 1108–1118, Dec. 2014.

[15] Z. H. Chen, K. L. Huang, S. Q. Liu, and H. Y. Wang, "Preparation and characterization of spinel $LiMn_2O_4$ nanorods as lithium-ion battery cathodes," *Trans. Nonferrous Met. Soc. China*, vol. 20, no. 12, pp. 2309–2313, Dec. 2010.

[16] J. H. Kim, S. T. Myung, C. S. Yoon, S. G. Kang, and Y. K. Sun, "Comparative study of $LiNi_{0.5}Mn_{1.5}O_{4-\delta}$ and $LiNi_{0.5}$ $Mn_{1.5}$ $O_4$ Cathodes Having Two Crystallographic Structures: Fd3m and $P4_332$," *Chem. Mater.*, vol. 16, pp. 906–914, Feb. 2004.

[17] A. Manthiram, K. Chemelewski, and E. S. Lee, "A perspective on the high-voltage $LiMn_{1.5}Ni_{0.5}O_4$ spinel cathode for lithium-ion batteries," *Energy Environ. Sci.*, vol. 7, no. 4, pp. 1339–1350, 2014.

[18] Q. Zhong, A. Bonakclarpour, M. Zhang, Y. Gao, and J. R. Dahn, "Synthesis and electrochemistry of $LiNi_x$ $Mn_{2-x}O_4$," *J. Electrochem. Soc.*, vol. 144, no. 1, pp. 205–213, 1997.

[19] J. H. Kim, S. T. Myung, and Y. K. Sun, "Molten salt synthesis of $LiNi_{0.5}Mn_{1.5}$ $O_4$ spinel for 5 V class cathode material of Li-ion secondary battery," *Electrochim. Acta*, vol. 49, no. 2, pp. 219–227, Jan. 2004.

[20] T. Yang, K. Sun, Z. Lei, N. Zhang, and Y. Lang, "The influence of holding time on the performance of $LiNi_{0.5}Mn_{1.5}O_4$ cathode for lithium ion battery," *J. Alloys Compd.*, vol. 502, no. 1, pp. 215–219, Jul. 2010.

[21] L. Wang, H. Li, X. Huang, and E. Baudrin, "A comparative study of Fd-3m and $P4_332$ 'LiNi$_{0.5}$Mn$_{1.5}$O$_4$," *Solid State Ionics*, vol. 193, no. 1, pp. 32–38, Jun. 2011.

[22] J. S. *rt al.*, "Role of oxygen vacancies on the performance of Li [$Ni_{0.5-x}$ $Mn_{1.5+x}$] $O_4$ (x = 0, 0.05, and 0.08) Spinel Cathodes for Lithium-Ion Batteries," *Chem. Mater.*, vol. 24, no. 15, pp. 3101–3109, Jul. 2012.

[23] M. A. Kebede, N. Kunjuzwa, C. J. Jafta, M. K. Mathe, and K. I. Ozoemena, "Solution-combustion synthesized nickel-substituted spinel cathode materials ($LiNi_xMn_{2-x}O_4$ ; $0 \leqslant x \leqslant 0.2$) for lithium ion battery: enhancing energy storage , capacity retention, and lithium ion transport," *Electrochim. Acta*, vol. 128, pp. 172–177, May 2014.

[24] H. W. Choi, S. J. Kim, Y. H. Rim, and Y. S. Yang, "Effect of Lithium Deficiency on Lithium-Ion Battery Cathode $Li_xNi_{0.5}Mn_{1.5}O_4$," *J. Phys. Chem. C.*, vol. 119, no. 49, pp. 27 192–27 199, Nov. 2015.

[25] G. C. Allen and M. Paul, "Chemical characterization of transition metal spinel-type oxides by infrared spectroscopy," *Appl. Spectrosc.*, vol. 49, no. 4, pp. 451–458, Apr. 1995.

[26] B. Ammundsen, G. R. Burns, M. S. Islam, H. Kanoh, and J. Rozière, "Lattice dynamics and vibrational spectra of lithium manganese oxides: A computer simulation and spectroscopic study," *J. Phys. Chem. B*, vol. 103, no. 25, pp. 5175–5180, Jun. 1999.

[27] Y. Zhao, C. Ma, and Y. Li, "One-step microwave preparation of a $Mn_3O_4$ nanoparticles/exfoliated graphite composite as superior

anode materials for Li-ion batteries," *Chem. Phys. Lett.*, vol. 673, pp. 19–23, Apr. 2017.

[28] H. L. *et al.*, "Morphological Evolution of High-Voltage Spinel $LiNi_{0.5}Mn_{1.5}O_4$ Cathode Materials for Lithium-Ion Batteries: the Critical Effects of Surface Orientations and Particle Size," *ACS Appl. Mater. Interfaces*, vol. 8, no. 7, pp. 4661–4675, Jun. 2016.

[29] B. H. *et al.*, "The effect of nanocrystallinity on the electrochemical performance of $LiMn_2O_4$ cathode syntetized by modified sol-gel method," *Solid State Ionics*, vol. 262, no. 7, pp. 9–13, Sep. 2014.

[30] C. M. Julien, F. Gendron, A. Amdouni, and M. Massot, "Lattice vibrations of materials for lithium rechargeable batteries. VI: Ordered spinels," *Mater. Sci. Eng. B*, vol. 130, no. 7, pp. 41–48, Jun. 2006.

[31] N. Amdouni, K. Zaghib, F. Gendron, a. Mauger, and C. M. Julien, "Structure and insertion properties of disordered and ordered $LiNi_{0.5}Mn_{1.5}O_4$ spinels prepared by wet chemistry," *Ionics*, vol. 12, no. 2, pp. 117–126, Jun. 2006.

[32] J. Yang, X. Han, X. Zhang, F. Cheng, and J. Chen, "Spinel $LiNi_{0.5}Mn_{1.5}O_4$ cathode for rechargeable lithiumion batteries: Nano vs micro, ordered phase ($P4_332$) vs disordered phase (Fd3m)," *Nano Res.*, vol. 6, no. 9, pp. 679–687, Sep. 2013.

[33] C. M. Julien, M. Massot, and C. Poinsignon, "Lattice vibrations of manganese oxides part I . periodic structures," *Spectrochim. Acta*, vol. 60, pp. 689––700, Feb. 2004.

[34] T. F. Yi, Z. K. Fang, Y. Xie, Y. R. Zhu, and L. Y. Zang, "Synthesis of $LiNi_{0.5}Mn_{1.5}O_4$ cathode with excellent fast charge-discharge performance for lithium-ion battery," *Electrochim. Acta*, vol. 147, pp. 250–256, Nov. 2014.

[35] H. Liu, R. Kloepsch, J. Wang, M. Winter, and J. Li, "Truncated octahedral $LiNi_{0.5}Mn_{1.5}O_4$ cathode material for ultralong-life lithium-ion battery: Positive (100) surfaces in high-voltage spinel system," *J. Power Sources*, vol. 300, pp. 430–437, Dec. 2015.

[36] K. R. Chemelewski, E. S. Lee, W. Li, and A. Manthiram, "Factors Influencing the Electrochemical Properties of High-Voltage Spinel Cathodes: Relative Impact of Morphology and Cation Ordering," *Chemistry of Materials*, vol. 25, no. 14, pp. 2890–2897, Jun. 2013.

[37] S. H. Y. *et al.*, "Improvement of the high-rate discharge capability of phosphate-doped spinel $LiMn_2O_4$ by a hydrothermal method," *Electrochim. Acta*, vol. 55, no. 8, pp. 2972–2977, Mar. 2010.

[38] J. M. Tarascon and D. Guyomard, "Li metal-free rechargeable batteries based on $Li_{1+x}Mn_2O_4$ Cathodes (0<x<1) and Carbon Anodes," *Journal of electrochemical society*, vol. 138, no. 10, pp. 2864–2868, 1991.

[39] D. L. *et al.*, "Spinel materials for high-voltage cathodes in Li-ion batteries," *RSC Adv.*, vol. 4, pp. 154–167, Nov. 2014.

[40] M. Hu, X. L. Pang, and Z. Zhou, "Recent progress in high-voltage lithium ion batteries," *AJ. Power Sources*, pp. 229–242, Sep. 2013.

[41] P. G. *et al.*, "Microwave rapid preparation of $LiNi_{0.5}Mn_{1.5}O_4$ and the improved high rate performance for lithium-ion batteries," *Electrochim. Acta*, vol. 100, pp. 125–132, Jun. 2013.

[42] A. C. *et al.*, "$LiNi_{0.5}Mn_{1.5}O_4$ t hick-film electrodes prepared by electrophoretic deposition f or use i n high v oltage l ithium-ion batteries," *J. Power Sources*, vol. 158, no. 1, pp. 583–590, Jul. 2006.

[43] Y. H. I. *et al.*, "Epitaxial growth of $LiMn_2O_4$ Thin Films by Chemical Solution Deposition for Multilayer Lithium-Ion Batteries," *J. Phys. Chem. C*, vol. 118, no. 34, pp. 19 540–19 547, Aug. 2014.

[44] C. J. Jafta, M. K. Mathe, N. Manyala, W. D. Roos, and K. I. Ozoemena, "Microwave-Assisted Synthesis of High-Voltage Nanostructured $LiMn_{1.5}Ni_{0.5}O_4$ Spinel: Tuning the $Mn^{3+}$ Content and Electrochemical Performance," *ACS Appl. Mater. Interfaces*, vol. 5, no. 15, pp. 7592–7598, Jul. 2013.

[45] K. Amine, H. Tukamot, H. Yasuda, and Y. Fujita, "Preparation and electrochemical investigation of $LiMn_{2-x}Me_xO_4$ (Me: Ni, Fe, and x = 0.5, 1) cathode materials for secondary lithium batteries," *J. Power Sources*, vol. 68, no. 2, pp. 604–608, Oct. 1997.

[46] H. Z. *et al.*, "Preparation and Characterization of Ultralong Spinel Lithium Manganese Oxide Nanofiber Cathode via Electrospinning Method," *Electrochim. Acta*, vol. 152, no. 25, pp. 274–279, Jan. 2015.

[47] X. X. *et al.*, "Synthesis of single-crystalline spinel $LiMn_2O_4$ Nanorods for lithium-ion batteries with high rate capability and long cycle life," *Chem. - A Eur. J.*, vol. 20, no. 51, pp. 217 125––17 131, Oct. 2014.

[48] Q. C. Z. *et al.*, "An Electrochemical Impedance Spectroscopic Study of the Electronic and Ionic Transport Properties of Spinel $LiMn_2O_4$," *J. Phys. Chem.*, vol. 114, no. 18, pp. 8614–8621, Apr. 2010.

[49] J. Bisquert, G. Garcia, F. Fabregat, and P. R. Bueno, "Theoretical models for ac impedance of finite diffusion layers exhibiting low frequency dispersion," *J. Electroanal. Chem.*, vol. 475, no. 2, pp. 152–163, Oct. 1999.

[50] B. H. *et al.*, "Determination of effective capacitance and film thickness from constant-phase-element parameters," *Electrochim. Acta J.*, vol. 55, no. 21, pp. 6218–6227, Aug. 2010.

[51] F. C. *et al.*, "Enhanced electrochemical performances of 5 V spinel $LiMn_{1.58}Ni_{0.42}O_4$ cathode materials by coating with $LiAlO_2$," *J. Power Sources*, vol. 239, pp. 181–188, Oct. 2013.

[52] M. M. *et al.*, "Improved cycling and rate performance of sm-doped $LiNi_{0.5}Mn_{1.5}O_4$ cathode materials for 5 v lithium ion batteries," *Appl. Surf. Sci.*, vol. 290, pp. 412–418, Jan. 2014.

[53] H. W. *et al.*, "Excellent stability of spinel $LiMn_2O_4$-based cathode materials for lithium-ion batteries.," *Electrochim. Acta*, vol. 177, pp. 290–297, Sep. 2015.

[54] M. Kunduraci, J. F. Sharab, G. G. Amatucci, and Other, "High-Power nanostructured $LiMn_{2-x}Ni_xO_4$ High-Voltage Lithium-Ion Battery Electrode Materials: Electrochemical Impact of Electronic Conductivity and Morphology," *Chem. Mater*, vol. 18, no. 15, pp. 3585–3592, Jul. 2006.

[55] M. Kunduraci, J. F. Sharab, and G. G. Amatucci, "High Rate Micron-Sized Ordered $LiNi_{0.5}Mn_{1.5}O_4$," *J. Electrochem. Soc*, vol. 157, no. 8, pp. 925–931, Jun. 2010.